Cancer Imaging (2013) **13(1),** 53–62
DOI: 10.1102/1470-7330.2013.0006

ORIGINAL ARTICLE

Whole-body diffusion-weighted magnetic resonance imaging at 3 Tesla for early assessment of treatment response in non-Hodgkin lymphoma: a pilot study

Katja De Paepe[a], Charlotte Bevernage[a], Frederik De Keyzer[a], Pascal Wolter[b], Olivier Gheysens[c], Ann Janssens[d], Raymond Oyen[a], Gregor Verhoef[d], Vincent Vandecaveye[a]

[a]Department of Radiology, University Hospitals Leuven, Belgium; [b]Department of General Medical Oncology, University Hospitals Leuven, Leuven Cancer Institute, Belgium; [c]Department of Nuclear Medicine, University Hospitals Leuven, Belgium; [d]Department of Haematology, University Hospitals Leuven, Belgium

Corresponding address: Vincent Vandecaveye; MD, PhD, Department of Radiology, University Hospitals Leuven, Herestraat 49, 3000 Leuven, Belgium.
Email: vincent.vandecaveye@uz.kuleuven.ac.be

Date accepted for publication 20 November 2012

Abstract

Objective: To evaluate 3 Tesla (T) whole-body diffusion-weighted magnetic resonance imaging (WB DWI) for early treatment assessment in aggressive non-Hodgkin lymphoma (NHL). **Methods:** Fourteen patients with NHL treated with standard chemotherapy underwent 3-T WB DWI before and 2 and 4 weeks during treatment, using *b*-values of 0–1000 s/mm^2 from which the apparent diffusion coefficient (ADC) was calculated. Patient follow-up (average 20.3 months, range 15–23 months) was the reference standard. Volume and ADC changes between baseline and 2 weeks (Vratio$_{2w}$, ADCratio$_{2w}$) and 4 weeks (Vratio$_{4w}$, ADCratio$_{4w}$) of responding and non-responding lesions (lymph node and organ lesions) were compared using Mann–Whitney U tests. The per patient values of Vratio$_N$ and ADCratio$_N$ to predict progression-free survival were determined with a log-rank test. **Results:** Eight patients showed complete remission and 6 showed tumour progression. The ADCratio$_{2w}$ and ADCratio$_{4w}$ differed significantly in lesions showing tumour progression versus complete remission (ADCratio$_{2w} = 4 \pm 21\%$ versus $119 \pm 68\%$; ADCratio$_{4w} = 18 \pm 61\%$ versus $155 \pm 78\%$; both $P < 0.0001$); the Vratio$_{2w}$ and Vratio$_{4w}$ did not ($P > 0.05$). Per body region, the ADCratio$_{2w}$ showed a negative predictive value of 100% and positive predictive value of 86%. Per patient, the ADCratio$_{2w}$ and ADCratio$_{4w}$ correlated significantly with progression-free survival ($P < 0.05$). **Conclusion:** 3-T WB DWI with ADC quantification may enable early treatment assessment of aggressive NHL.

Keywords: *Whole-body imaging; diffusion-weighted magnetic resonance imaging; non-Hodgkin lymphoma; chemotherapy; treatment outcome.*

Introduction

Lymphomas are a heterogeneous group of malignancies arising from lymphoid tissue, with varied clinical and biological features classified according to morphologic, immunophenotypic and genetic features. The most common type of non-Hodgkin lymphoma (NHL) is diffuse large B-cell lymphoma (DLBCL), which accounts for about 30% of lymphoid neoplasms[1]. T-cell lymphomas (TCL) represent about 12% of NHL. Aggressive or high-grade NHL is defined as a subgroup that shows severe clinical symptoms and rapid disease progression if untreated.

The prognosis and outcome for patients with aggressive NHL are influenced by accurate staging at diagnosis and correct and timely recognition of treatment response. [^{18}F]Fluorodeoxyglucose (FDG)-positron emission tomography (PET) is being increasingly used instead of contrast-enhanced computed tomography (CT) for the staging and treatment follow-up of aggressive NHL and efforts have been made to standardize the performance

and interpretation criteria of FDG-PET for staging and treatment assessment[2]. Compared with CT alone, FDG-PET/CT shows improved differentiation of post-treatment residual tumoural disease from post-treatment fibrosis. Although it was shown that interim PET during treatment effectively predicts the outcome for patients with DLBCL, the clinical value of early treatment evaluation with FDG-PET regarding patient management is not yet entirely clear[3–5].

Magnetic resonance imaging (MRI) is emerging as an efficient whole-body (WB) imaging modality combining sequences with adequate spatial and contrast resolution. However, using only conventional imaging sequences makes WB MRI, similar to CT, largely dependent on morphologic and size-related criteria for lesion characterization, potentially decreasing its value for nodal characterization or (early) treatment assessment[6]. Assessment of T2 signal intensity (SI) may be of additional use to differentiate post-treatment residual fibrotic masses and differentiate fibrotic tissue from masses at risk for relapse. However, previous studies suggest that optimal accuracy may only be reached 6 months after the end of treatment but clinically relevant decisions must be taken in the early stages of treatment[7,8]. Several studies have indicated the additional value of functional MR techniques to conventional MRI for lesion characterization and early treatment assessment in various solid tumours[9–11]. Diffusion-weighted MRI (DWI) characterizes tissue by probing changes in random water molecule mobility related to differences in the tissue microstructure. These lead to changes in SI with increasing diffusion sensitization (*b*-value), which can be quantified by the apparent diffusion coefficient (ADC), allowing viable tumour to be differentiated from necrosis and inflammation irrespective of the underlying lesion morphology[12]. Recent and rapid technological developments have made the technique suitable for WB imaging in addition to morphologic imaging[13–15].

Recently, studies at 1.5 T investigated the feasibility of WB DWI for early treatment assessment of lymphoma[16]. Also, preliminary data indicate that DWI may be used as a response marker very early during treatment for lymphoma[17]. The aim of this pilot study was to evaluate WB DWI at 3 T performed at 2 and 4 weeks after the start of treatment for early assessment of treatment response in aggressive NHL.

Designs and methods

Patients

The study was approved by the local ethics committee and all patients gave written informed consent before the study. Patients with histological proof of NHL and scheduled for standard chemotherapy were included. Exclusion criteria were history of previous other malignancy or haematologic disorder, contraindications to MRI (such as pacemaker or claustrophobia) and pregnancy.

Fifteen consecutive patients who met these inclusion criteria with histopathologically proven NHL (13 de novo developed DLBCL and 2 TCL) were included in this prospective single-centre study between October 2008 and March 2009. One patient with DLBCL did not complete the treatment schedule due to treatment-induced toxicity and was consequently excluded. The following details for the 14 remaining patients are shown in Table 1: the lymphoma (sub)type, disease location, Ann Arbor staging and international prognostic index (IPI) score calculated from the patient's age (>60 years), Eastern Cooperative Oncology Group (ECOG) scale (patient's performance ranging from asymptomatic to chronically bedridden), blood level of lactate dehydrogenase (LDH), number of extranodal disease sites and disease stage. Routine pretreatment evaluation and Ann Arbor staging were based on clinical examination, laboratory screening, PET/CT, lymph node excisional biopsy

Table 1 **Histological diagnosis, lymphoma subtype, Ann Arbor stage, IPI score, and treatment schedule at the time of patient inclusion**

Patient	Histology	Subtype	Ann Arbor classification	Nodal involvement	Organ involvement	IPI	Treatment
1	DLBCL	GCB	II	Infradiaphragmatic		1	R-CHOP$_{14}$
2	DLBCL	ABC	IIE	Infradiaphragmatic	Stomach	3	R-CHOP$_{14}$
3	DLBCL	ABC	IV	Infradiaphragmatic	Skeletal	2	R-CHOP$_{14}$
4	DLBCL	GCB	IV	Infradiaphragmatic	Skeletal	3	R-CHOP$_{21}$
5	DLBCL	ABC	IV	Infra-supradiaphragmatic	Skeletal, uterine	4	R-CHOP$_{21}$
6	DLBCL	GCB	IIIE	Infra-supradiaphragmatic	Caecum	1	R-CHOP$_{14}$
7	DLBCL	GCB	III	Infra-supradiaphragmatic		3	R-CHOP$_{21}$
8	DLBCL	GCB	IV	Infra-supradiaphragmatic	Skeletal	5	R-CHOP$_{14}$
9	TCL	ALCL	I	Supradiaphragmatic		0	CHOP$_{21}$
10	DLBCL	GCB	II	Infradiaphragmatic		2	R-CHOP$_{21}$
11	DLBCL	ABC	IV	Supradiaphragmatic	Skeletal	2	R-CHOP$_{21}$
12	DLBCL	GCB	II	Infradiaphragmatic		1	R-CHOP$_{21}$
13	DLBCL	GCB	IV	None	Skeletal	3	R-CHOP$_{21}$
14	TCL	extranodal-NK	IV	None	Skeletal	4	CHOP$_{21}$

ABC, activated B-cell phenotype; ALCL, anaplastic large cell lymphoma; extranodal-NK, extranodal natural killer cell; GCB, germinal centre B-cell phenotype.

and bone marrow biopsy. Clinical response assessment was based on PET/CT examinations after 3 cycles for study purposes, conforming to the protocol of ongoing clinical trials at our centre, and at the end of the chemotherapy schedule, according to international guidelines[2].

For DLBCL, the treatment schedule consisted of 6–8 cycles of R-CHOP (rituximab 375 mg/m^2 intravenous (iv) day 1; cyclophosphamide 750 mg/m^2 iv day 1; vincristine 1.4 mg/m^2 iv day 1; doxorubicin 50 mg/m^2 iv day 1; prednisone 100 mg by mouth days 1–5); 5 patients received a 2-weekly schedule of R-CHOP (R-CHOP$_{14}$, R-CHOP plus addition of growth factor support, Pegfilgrastim (Neulasta®) 6 mg subcutaneous injection, day 2) and 7 patients received a 3-weekly schedule (R-CHOP$_{21}$). The 2 patients with TCL were treated with CHOP, not including rituximab.

In addition to routine diagnostic procedures, 3-T WB DWI was performed before and 2 and 4 weeks after the initiation of treatment. All MRI studies were well supported by the patients and were of sufficient quality to allow analysis.

Imaging technique

WB MRI

WB imaging, covering the brain down to the proximal one-third of the upper legs, was performed on a 3-T MRI scanner (Achieva; Philips, Best, The Netherlands) with parallel radiofrequency transmission. The application of parallel radiofrequency transmission significantly improves image quality with respect to signal homogeneity and fat suppression[18]. Images were acquired using the built-in Q-body coil, which does not allow parallel imaging; however, the absence of surface coils maximizes patient comfort and minimizes patient positioning time.

Conventional WB MRI as anatomical reference for the WB DWI images and for measurement of lesion volume consisted of a coronal T2-weighted short tau inversion recovery (STIR) sequence acquired in 4 imaging stations. Each imaging station consisted of 26 slices; 5.6 mm slice thickness, intersection gap of 0.6 mm, field of view (FoV) of 470 × 270 mm, voxel resolution of 1.5 × 2 × 5.6 mm and repetition time (TR)/echo time (TE) of 8102/70 ms. Sequence time was 2 min and 58 s per imaging station.

Free-breathing WB DWI was acquired using 7 identical imaging stations in the transverse plane. Each imaging station consisted of 32 slices, 5.5 mm slice thickness, intersection gap of 0.1 mm, FoV of 420 × 323 mm, voxel resolution of 4 × 4 × 5.5 mm, 3 averages acquired and TR/TE of 6204/60 ms. Sequence time was 2 min and 29 s per imaging station. Two *b*-values were applied in 3 orthogonal directions and combined ($b = 0$ and 1000 s/mm^2) from which ADC maps were automatically calculated. After acquisition, the transverse DW images were coronally reformatted using the built-in multiplanar reformatting (MPR) software and combined into a single stack of coronal WB DWI images with a slice thickness of 5 mm.

PET/CT

Patients fasted for 6 h before the PET/CT examination (Biograph 40 TruePoint with TrueV, Siemens Medical Solutions, Erlangen, Germany). Single-section WB spiral CT (40-slice Siemens Sensation, 85 mAs, 120 kV, slice thickness 5 mm, collimation 24 × 1.2 mm, table feed 23 mm/rotation) was performed after intravenous injection of 120 ml of a contrast agent containing 300 mg iodine/ml. PET/CT images were acquired 60 min after intravenous administration of FDG at an average dose of 302.6 MBq (range 220–388 MBq). PET was performed with an optimal in-plane resolution of 4.5 mm and an axial FoV of 216 mm. PET images were corrected for attenuation using the CT data.

Image analysis

Lesion identification and imaging correlation

Lymph node and organ lesions diagnosed as malignant by pretherapeutic clinical and imaging (PET/CT) assessment were included for evaluation by WB DWI and WB STIR.

In total, 138 lesions corresponding to 61 regions were delineated and analysed. Of the 138 lesions, 80 were lymphadenopathies (mean longest axis diameter 2.5 ± 2.3 cm, including 1 tonsillar lymphoma location (longest axis diameter 1.3 cm)), 3 lesions were at a visceral location (stomach, caecum and uterus, mean longest axis diameter 7.7 ± 1.2 cm) and 55 lesions were located in the bone marrow (mean longest axis diameter 2.7 ± 1.5 cm). At baseline, these target lesions were first identified and located on the coronal reformatted WB DWI acquired with $b = 1000$ s/mm^2 (b1000 image) and WB STIR and correlated with FDG-positive lesions on the coronal PET/CT images. After lesion annotation on the coronal images, the lesions were automatically identified by the software on the corresponding co-registered transverse b0 and b1000 images. Lesions were also topographically annotated by their slice position and anatomical position. These target lesions for longitudinal follow-up were identified on WB DWI and WB STIR at 2 and 4 weeks follow-up by visual correlation and correlation of slice positions with the baseline examination.

WB STIR

Volumetric analysis was performed on the WB STIR images by 2 readers in consensus (KDP and RO). On these T2-weighted images, the signal of background tissue (fat, muscle, bone) is suppressed and lymph node and organ lesions are depicted as hyperintense structures. For each lesion, contours were drawn around the lesion border at each slice position and lesion volume was

calculated with the following equation: (Σsurface at each slice position) × (slice thickness + intersection gap). The volume changes (Vratio$_N$ in %) for each lesion between the baseline and the 2 and 4 weeks time points were calculated using the formula $V\text{ratio}_N = \{(V_N - V_B)/V_B\} \times 100$ where V_B represents the pretreatment volume and V_N represents the volume at either 2 or 4 weeks after the start of treatment.

WB DWI

After correct lesion localization, the WB DWI images were quantitatively interpreted by 2 readers in consensus (CB and VV), blinded from clinical and other imaging data. For quantitative assessment, a similar approach was used as described in the literature[19]. Regions of interest (ROIs) were placed over lymphoma localizations on the b0 images and automatically copied to the other *b*-value images by the software. For solid nodal and extranodal lesions, the ROIs were placed over the entire lesion. In the case of obvious solid and necrotic components on the DW images, ROIs were placed on the solid tumoural components according to their signal heterogeneity on the b1000 images[19].

Native high *b*-value images allow the separate tissue components to be identified. Currently, there is no agreement as to which *b*-value best delineates intact tumoural tissue from necrosis or background tissue. Therefore, for this study, the native b1000 images were chosen to identify solid tumoural areas from background or necrosis as it is most likely that the suppression of T2 shine-through effects in necrosis or fluid-containing regions is most effective and that the volume of solid tumoural tissue cannot be overestimated due to remnant signal in necrotic areas.

For each lesion, all ROIs were combined into a single ROI and the average SI was then calculated for each *b*-value. These averaged SI values were then used to calculate the ADC (in mm^2/s) using the following equation: $\text{ADC} = (-1/1000) \times \ln(\text{SI}_{b1000}/\text{SI}_{b0})$ where SI_{b1000} and SI_{b0} are the SI measured on the b1000 and b0 images, respectively.

Subsequently, for early treatment follow-up at 2 and 4 weeks after the start of chemotherapy, the ADC changes (ADCratio$_N$, in %) for each lesion between baseline and 2 and 4 weeks were calculated using the following formula: $\text{ADCratio}_N = \{(\text{ADC}_N - \text{ADC}_B)/\text{ADC}_B\} \times 100$ where ADC_B represents the pretreatment ADC value and ADC_N represents the ADC at either 2 or 4 weeks after the start of treatment.

PET/CT

PET images were qualitatively evaluated. The standard uptake value (SUV) is not routinely used at our institution and was not applied for determination of PET results. Response assessment was performed according to the recommendations of the imaging subcommittee of the international harmonization project in lymphoma[2]. The extent and intensity of all foci of abnormal uptake were evaluated using a 3-point scale (1, low; 2, moderate; 3, high) within each lymphatic area, organ and skeletal region. Negative was defined as having no residual uptake or as having a single residual site of uptake with an intensity of 1. Positive was defined as having at least 1 residual site with an intensity score of at least 2 or the presence of at least 2 residual sites with any extent and intensity score.

Reference standard: treatment outcome

For clinical follow-up, patients underwent PET/CT after completion of treatment and were further followed by the treating physician at the outpatient clinic every 3 months during the time of study follow-up. Imaging studies, CT and/or PET/CT, were performed at the discretion of the treating physician when tumour progression or relapse was suspected. The total patient follow-up time was on average 20.3 months (range 15–23 months). Progression-free survival (PFS) was defined as the time between the end of therapy and the time of disease progression in case of tumour recurrence, or between the end of therapy and the end of follow-up in case of clinical remission (CR). CR was defined as the absence of all detectable clinical evidence of disease and disease-related symptoms, absent FDG uptake in nodal and extranodal residual masses, and absence of lymphoma infiltrations on repeat bone marrow biopsy (in case of bone marrow involvement before treatment). Tumour recurrence was defined as any new or persistent lesions of more than 1.5 cm in any axis on follow-up CT and/or any persisting or new lesions with pathologic focal FDG uptake not attributable to inflammation, confirmed by biopsy and histopathology.

Statistical analysis

Statistical analysis was done using Analyse-it 2.12 (Analyse-it Software, Ltd., Leeds, United Kingdom) and SPSS 11.0 for Windows (SPSS, Chicago, IL, US) A P-value < 0.05 was considered statistically significant. The ADCratio$_N$ and Vratio$_N$ of nodal and extranodal lymphoma locations showing CR versus recurrence during follow-up were compared with the Mann–Whitney U test. If a statistical difference was found, a further receiver operating curve (ROC) analysis with area under the curve (AUC) was used to investigate the discriminatory capability of the ADCratio$_N$ and Vratio$_N$. After determining the optimal cut-off (giving equal weight to sensitivity and specificity), the sensitivity, specificity, accuracy, positive predictive value (PPV) and negative predictive value (NPV) of the imaging parameters were determined per body region taking into account the lesions with lowest ratio$_N$ in each body region. For each of these values, the 95% binomial confidence interval (CI) was also provided.

On a per patient base, survival analysis was performed towards the PFS using the Kaplan–Meier product-limited (actuarial) method. The ADC ratio was dichotomized using the same threshold as for the per body region analysis, taking into account the lesion with the lowest ADC ratio per patient. The statistical significance of differences between curves was compared with the log-rank test for the imaging parameters and IPI score.

Results

Treatment outcome

Eight of the 14 patients (57%) showed CR at the end of follow-up. Three patients (21%) showed persisting or progressive disease at the end of standard treatment. Treatment intensification, which consisted of radiotherapy of the persisting disease site, was possible in only 1 patient (7%), leading to CR in this patient. In the other 2 patients (14%), rapid disease progression was noted followed by death. Three patients showed tumour recurrence during the follow-up period. Histologically proven tumour relapse occurred in the brain in 1 patient at 8 months after treatment, not related to previous affected sites; in nodal stations and spine in 1 patient at 12 months after treatment, related to previously affected sites; and in nodal stations in 1 patient at 6 months, also related to previously affected sites. All 3 patients received salvage treatment consisting of R-DHAP (rituximab, dexamethasone, cytarabine, cisplatin) and/or radiotherapy. One of these 3 patients died during the follow-up period, 1 patient went into CR and 1 patient was alive under palliative care.

WB STIR

Lesion-based analysis

Per lesion, $V\text{ratio}_{2w}$ and $V\text{ratio}_{4w}$ showed no significant difference between lesions showing persisting or recurrent disease compared with lesions with CR ($V\text{ratio}_{2w} = -51 \pm 32\%$ versus $-71 \pm 34\%$; $V\text{ratio}_{4w} = -56 \pm 46\%$ versus $-83 \pm 32\%$; both $P > 0.05$). Due to lack of statistical significance, further region- and patient-based analyses were not performed.

WB DWI

Lesion-based analysis

Per lesion, ADCratio_{2w} and ADCratio_{4w} were significantly different in lesions showing persisting or recurrent disease compared with lesions with CR. At 2 and 4 weeks during treatment, the ADC ratios compared with baseline were significantly lower in non-responding than in responding lesions ($\text{ADCratio}_{2w} = 4 \pm 21\%$ versus $119 \pm 68\%$; $\text{ADCratio}_{4w} = 18 \pm 61\%$ versus $155 \pm 78\%$; $P < 0.0001$) (Fig. 1).

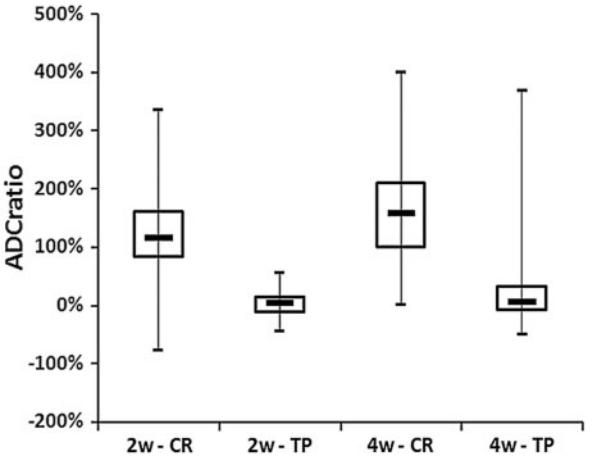

Figure 1 **Box-whisker plots for ADCratio_{2w} and ADCratio_{4w} between NHL localizations showing later remission (CR) versus later recurrence (tumour progression, TP). Box plots illustrate median (line inside box), interquartile range (box) and minimal and maximal values (lines extending below and above box). ADCratio_{2w} and ADCratio_{4w} values were significantly higher in NHL localizations showing remission during follow-up compared with NHL localizations with later recurrence.**

Region-based analysis

When we assigned the lesion with the lowest ADCratio_{2w} as representative of the respective region, a ROC analysis incorporating equal weighting to sensitivity and specificity calculated the optimal thresholds for ADCratio_{2w} and ADCratio_{4w} as 25% and 40%, respectively. Using these thresholds, the ADCratio_{2w} yielded a sensitivity for detection of CR of 100% (CI 74–100%), specificity of 90% (CI 70–99%), accuracy of 94% (CI 80–99%), NPV of 100% (CI 82–100%) and PPV of 86% (CI 57–98%). The ADCratio_{4w} showed a sensitivity of 83% (CI 52–98%), specificity of 91% (CI 71–99%), accuracy of 88% (CI 73–97%), NPV of 91% (CI 71–99%) and PPV of 83% (CI 52–98%) (Table 2).

Patient-based analysis

In the survival analysis, no significant differences in PFS could be found between the group with IPI score >1 compared with the group with IPI score ≤ 1 ($P = 0.6$). However, patients for whom ADCratio_{2w} and ADCratio_{4w} of all lesions were above these thresholds did show statistically longer PFS (ADCratio_{2w}, $P = 0.0002$; ADCratio_{4w}, $P = 0.005$) (Fig. 2). The ADCratio_{2w} correctly identified all 8 patients showing CR, and 5 of 6 patients with persisting disease or later recurrence as illustrated in Figs. 3 and 4. The ADCratio_{4w} correctly identified 7 of 8 patients with CR as illustrated in Fig. 5, and 5 of 6 patients with persisting disease or later recurrence, but misclassified 2 patients.

Table 2 **Accuracy of $ADCratio_{2w}$ and $ADCratio_{4w}$ per body region**

Per body region	$ADCratio_{2w}$	$ADCratio_{4w}$
Cut-off (%)	25	40
True-positive	12	10
False-positive	2	2
False-negative	0	2
True-negative	19	20
Sensitivity (%)	100	83
Specificity (%)	90	91
Accuracy (%)	94	88
NPV	100	91
PPV	86	83

Clinical PET/CT

PET/CT data were acquired at the time of diagnosis, after 3 cycles ($PET_{3cycles}$) of chemotherapy and at the end of treatment ($PET_{endtreatment}$). $PET_{3cycles}$ showed complete metabolic response in 7 of 8 patients with later CR and near-complete response with one residual hypermetabolic focus (intensity grade >1) in 1 of these 8 patients. Of the 6 patients with primary refractory disease or relapse, the $PET_{3cycles}$ showed at least 2 persistent lesions in 4 patients and complete metabolic remission in 2 patients.

$PET_{endtreatment}$ showed a complete metabolic response in 8 of 8 patients with CR at the end of follow-up. In the

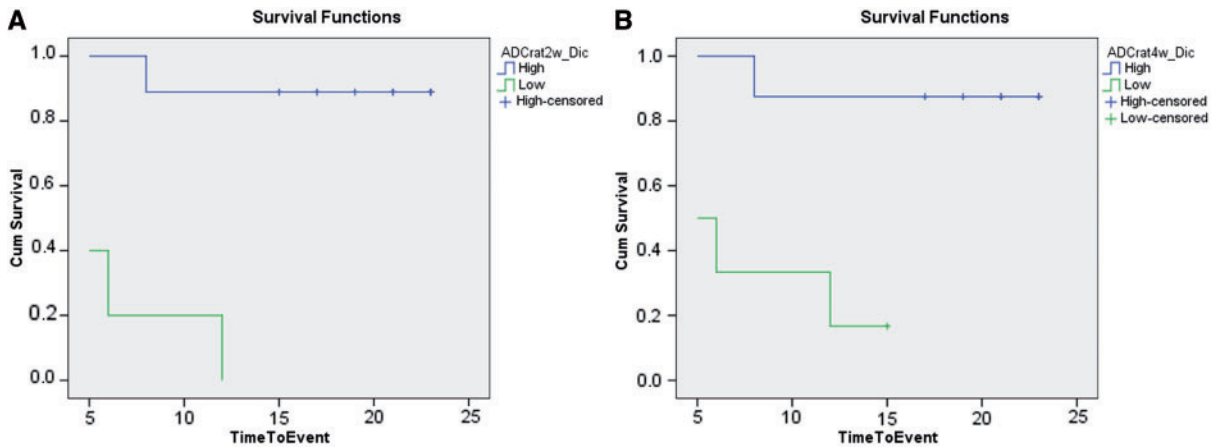

Figure 2 **Kaplan–Meier PFS curves for (A) $ADCratio_{2w}$ ($P = 0.0002$) and (B) $ADCratio_{4w}$ ($P = 0.005$). At both time points, ADC_{ratio} values above the threshold were indicative of a significantly longer PFS.**

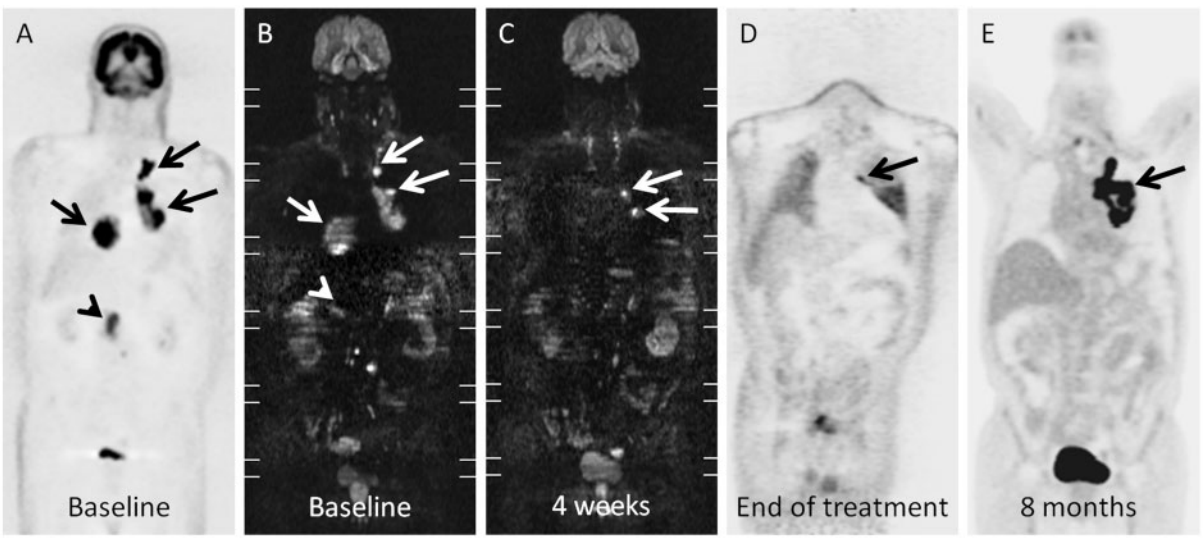

Figure 3 **(A) Baseline FDG-PET and (B) WB DWI b1000 image shows a patient with stage III NHL with mesenteric adenopathies (arrowhead), right and left hilar as well as left upper mediastinal adenopathies (arrows). (C) MPR coronal reformatted WB DWI b1000 image at 4 weeks during treatment shows persisting hyperintense areas in the left hilar adenopathies with an $ADCratio_{4w}$ below the threshold of 40%. (D) FDG-PET at end of treatment shows residual uptake in the left hilar area. (E) FDG-PET at 8 months after completion of treatment shows a large metabolic left hilar mass compatible with tumour relapse.**

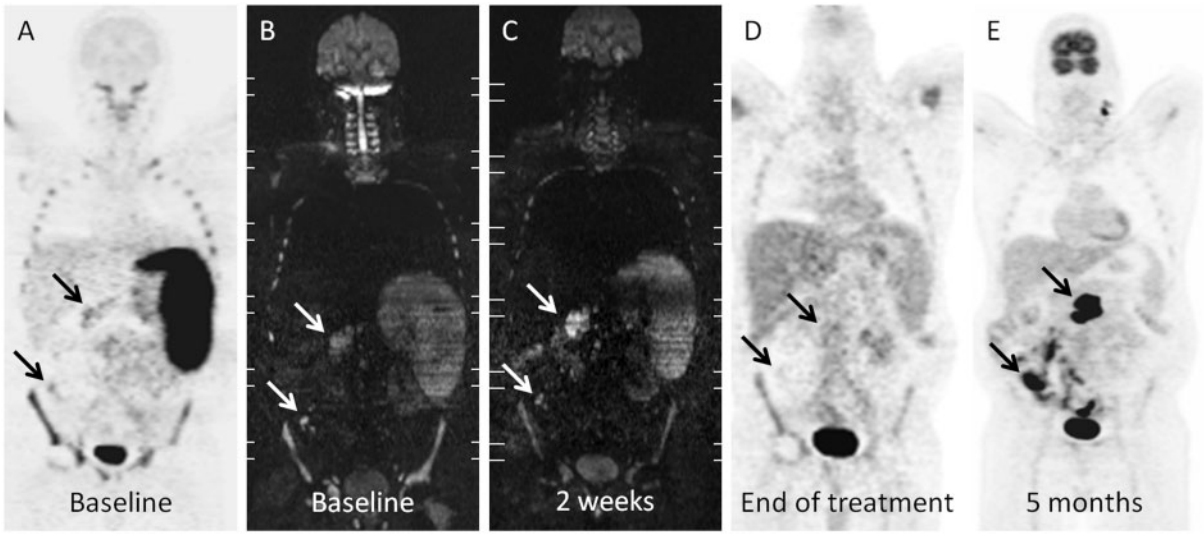

Figure 4 **(A) Baseline FDG-PET and (B) MPR coronal reformatted WB DWI b1000 images show a patient with stage IV NHL with tumoural involvement of mesenteric adenopathies (arrows), diffuse skeletal involvement and in the spleen. (C) MPR coronal reformatted WB DWI b1000 images 2 weeks during treatment show unchanged SI in the mesenteric adenopathies (arrows) with an ADC ratio below the threshold of 25%. (D) FDG-PET at the end of treatment shows faint uptake in the largest upper abdominal mesenteric deposit and no uptake in the smallest deposit in the right lower abdomen (arrows). (E) FDG-PET 5 months after end of treatment shows tumour relapse at the site of mesenteric adenopathies (arrows) and in the left upper neck lymph nodes.**

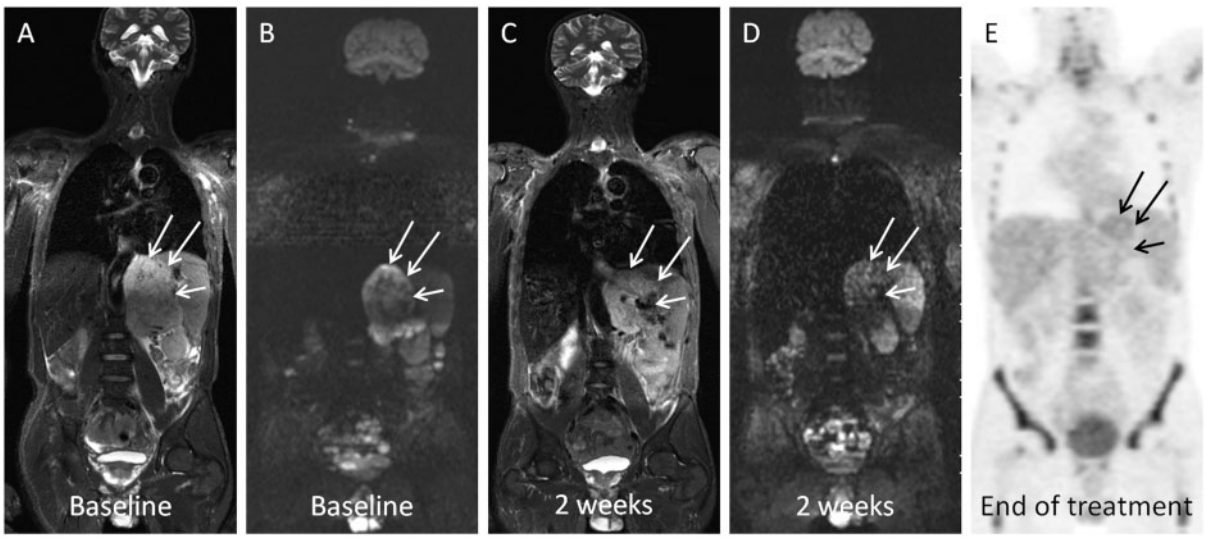

Figure 5 **(A) Baseline coronal T2-weighted STIR and (B) MPR coronal reformatted WB DWI b1000 images show large NHL localization in the mesentery of the left upper abdomen (arrows). (C) Coronal T2-weighted STIR image shows limited decrease in size of the mass at 2 weeks after start of treatment. (D) MPR coronal reformatted WB DWI b1000 images show nearly complete regression of b1000 SI in the mass corresponding to an $ADCratio_{2w}$ above the threshold of 25%. (E) FDG-PET at the end of treatment shows complete metabolic response. The patient is disease free at 23 months of follow-up.**

6 patients with primary refractory disease or relapse, $PET_{endtreatment}$ showed persistent disease in 4 patients and complete metabolic remission in 2 patients. Comparative data between the different DWI and FDG-PET time points are shown in Table 3.

Discussion

This pilot study investigated the value of 3-T WB DWI using the built-in body coil for early assessment of treatment response to standard chemotherapy in aggressive

Table 3 **Comparative table showing prediction of CR after treatment up to 2 years follow-up per patient for $ADCratio_{2w}$, $ADCratio_{4w}$ and FDG-PET/CT at 3 cycles and at the end of treatment**

Patient no.	Outcome*	$ADCratio_{2w}$	$ADCratio_{4w}$	$PET_{3cycles}$	$PET_{endtreatment}$
1	CR	−	-	-	-
2	CR	−	−	+ (FP)	−
3	TP	+	+	+	+
4	CR	−	+ (FP)	−	−
5	TP	− (FN)	− (FN)	− (FN)	− (FN)
6	CR	−	−	−	−
7	TP	+	+	+	+
8	CR	−	−	−	−
9	CR	−	−	−	−
10	CR	−	−	−	−
11	TP	+	+	− (FN)	− (FN)
12	TP	+	+	+	+
13	CR	−	−	−	−
14	TP	+	+	+	+

+, predicted as TP, −, predicted as CR; FP, false-positive; FN, false-negative.

NHL, correlated to a follow-up based reference standard. NHL localizations that responded well during patient follow-up showed a significantly higher $ADCratio_{2w}$ and $ADCratio_{4w}$ compared with non-responding lymphoma localizations. In contrast, changes in lesion volume failed to show significant differences between responding and non-responding lesions. It is known that a decrease in lesion size in response to cytotoxic agents often occurs in the delayed phase or may be absent due to the development of fibrosis making the differentiation between responders and non-responders difficult, especially in the early treatment phase. This potentially makes size-based imaging inefficient as an early marker for treatment response[20,21]. Cellular and vascular changes in response to cytotoxic treatment are known to precede changes in lesion size or occur when size changes are lacking, making DWI a potential early indicator of tumour chemosensitivity towards cytotoxic treatment[22].

In previous studies on breast cancer, primary and metastatic liver cancer, skeletal sarcoma, brain tumours and head and neck cancer, a substantial increase in ADC has been consistently correlated with successful treatment[19,23–27]. These ADC changes may relate to the induction of necrosis and apoptosis in response to cytotoxic treatment[28]. For NHL, the possible inverse correlation between ADC changes and tissue microdensity during treatment follow-up has been investigated by Huang et al.[29] in NHL xenografts. Treated tumour xenografts exhibited an increased ADC and had much lower cell density and cell proliferation and higher levels of apoptosis in comparison with non-treated controls. This is in concordance with a previous study using an animal glioma model in which biologically relevant outcome measures, such as cell kill and animal survival, correlated significantly with early changes in cellular density and mitotic index[27].

Recently, 2 studies investigated the feasibility of 1.5-T WB DWI for early treatment assessment of lymphoma. Lin et al.[16] found a significant increase in ADC in residual persisting masses after treatment, thereby potentially reducing the number of false-positives caused by size analysis alone. WB DWI findings were correlated to short follow-up and findings on PET/CT. In a second study, Wu et al.[17] noted a significant increase in ADC as early as 1 week after the start of chemotherapy and after 2 cycles of chemotherapy, and the PET/CT measured tumour metabolic activity and volume decrease at the same time. No significant difference was found in the study of Lin et al.[16] between the ΔADC of PET-positive and PET-negative regions, which were considered attributable to the small percentage of positive PET scans, and short time of follow-up.

In addition to these previous studies, we found a significant correlation between $ADCratio_N$, the eventual occurrence of tumour relapse and PFS during the 15–23 months of follow-up. In a study monitoring chemoradiation of head and neck cancer, DWI 2–4 weeks after the start of chemoradiation allowed prediction of the clinical response after 2 years of follow-up[19]. Similarly, DWI 3 weeks after the start of chemoradiation correlated with pretreatment DWI has been shown to predict time to progression and overall survival in patients with glioma[27].

All imaging techniques misclassified 1 patient with stage IV DLBCL, who reached remission on all target lesions but developed a biopsy-proven tumour relapse in the brain parenchyma during follow-up. In contrast, $ADCratio_{2w}$ correctly predicted tumour relapse in 1 patient with DLBCL who showed good response on FDG-PET after 3 cycles and at the end of treatment. However, these localizations showed lower FDG avidity on the pretreatment scan, possibly hampering adequate evaluation of treatment response. In a previous report, DLBCL glucose metabolism measured by SUV and ADC showed no correlation. Because SUV as a marker for tumour metabolism and ADC as a marker for tumour microstructure are different indices characterizing malignancy, both should be considered to provide complementary diagnostic information[30].

One of the potential difficulties with patient-based treatment assessment with WB DWI compared with assessment of a single lesion or organ system, as in head and neck cancers or brain tumours, is to correlate the early response of a multitude of separate tumoural localizations in a single patient to the eventual treatment outcome of that patient. In cytotoxic treatment of systemic disease such as NHL, a homogeneous response cannot be expected to occur in all lesions. This is illustrated in our patient population, where treatment failure was often based on insufficient response of a single or a few lesions even with the other localizations showing excellent treatment response. Therefore, the patient-based analysis was primarily based on the heterogeneity of response over all lesions, with the identification of the least responsive lesion being predictive for PFS. Simplified, analysis of patient outcome should aim at detection of lesions with the lowest ADC ratio during treatment, although this should still be confirmed in larger studies. This concept of heterogeneity of response also drives our choice for ROI delineation based on tumour heterogeneity, only including the b1000 hyperintense, or suspected solid, tumoural areas. Early treatment assessment should aim at timely selection of non-responders, in whom small surviving intratumoural deposits may be responsible for tumour relapse while large parts of the tumour become necrotic. If whole lesion delineation was performed, lack of ADC changes in small surviving tumoural parts may have been masked by excessive ADC changes in the neighbouring responding tissues[19]. Nevertheless, we acknowledge that this methodology combining qualitative and quantitative interpretation should preferably be validated in larger studies.

A current issue is the need for time-consuming manual ROI delineations to calculate ADC values. Moreover, the calculated mean or median ADC ratio may not entirely reflect the intratumoural changes in response to treatment[31]. More automated evaluation methods incorporating tumour heterogeneity on a voxel or subvoxel level, such as functional diffusion maps (fDM), may have the added value of reflecting the intralesional heterogeneity of treatment response, thereby possibly improving diagnostic accuracy[31]. However, to our knowledge the fDM has not yet been applied for evaluation of multiple lesions in WB DWI. In addition, similar to a recent study of Horger et al.[32], we obtained reasonable accuracy by calculating changes in averaged ADC obtained from ROIs based on visual assessment of b1000 SI tumoural heterogeneity.

There were some limitations to this study. First, the number of patients was small, but the significant study findings provide a basis for more extensive studies integrating WB DWI in the early treatment assessment of aggressive NHL. Second, this study was performed on a 3-T system using the built-in body coil, which may limit the comparison or extrapolation of these results to other studies or systems with different field strength or coil set-up. Although the major disadvantage of using the built-in body coil is the inability to use parallel imaging to increase the signal to noise ratio and decrease artefacts, it enabled us to perform efficient WB imaging with maximal patient comfort and minimized time loss due to patient positioning. However, the availability of dedicated WB surface coil designs with large coverage in the *z*-axis is increasing and will likely become the standard method for WB imaging [33]. Nevertheless, our study shows the ability to perform WB imaging at 3 T with the built-in body coil may remain beneficial in case of patients with claustrophobia or high levels of discomfort or morbidity, e.g. in tumour-induced pain syndromes such as multifocal skeletal metastases.

Third, in this study no direct comparison of WB DWI and FDG-PET/CT at identical time points was performed. However, in the setting of this pilot study in a small patient group, we opted to minimize the additional burden to the patient by limiting the FDG-PET/CT scans to those required for routine clinical purposes in our centre. Nevertheless, we acknowledge that in further studies, scanning at similar and preferably early time points is advised to compare both imaging modalities and evaluate their potential synergistic value.

Conclusions

In this pilot study, WB DWI with the $ADCratio_{2w}$ and $ADCratio_{4w}$ allowed for early assessment of treatment response, correlating significantly with the PFS during an average 20 months of follow-up. Lower $ADCratio_{2w}$ and $ADCratio_{4w}$ values were indicative of worse treatment outcome. However, larger studies are required to further evaluate the potential role of WB DWI as an early biomarker in the treatment of aggressive NHL.

Conflict of interest

The authors have no conflicts of interest to declare.

References

[1] Flowers CR, Sinha R, Vose JM. Improving outcomes for patients with diffuse large B-cell lymphoma. CA Cancer J Clin 2010; 60: 393–408. PMid:21030533.

[2] Cheson BD, Pfistner B, Juweid ME, et al. Revised response criteria for malignant lymphoma. J Clin Oncol 2007; 25: 579–586. doi:10.1200/JCO.2006.09.2403. PMid:17242396.

[3] Safar V, Dupuis J, Jardin F, et al. Interim [^{18}F]fluorodeoxyglucose positron emission tomography scan in diffuse large B-cell lymphoma treated with anthracycline-based chemotherapy plus rituximab. J Clin Oncol 2012; 30: 184–190. doi:10.1200/JCO.2011.38.2648. PMid:22162590.

[4] Mikhaeel NG. Interim fluorodeoxyglucose positron emission tomography for early response assessment in diffuse large B cell lymphoma: where are we now? Leuk Lymphoma 2009; 50: 1931–1936. doi:10.3109/10428190903275610. PMid:20001245.

[5] Cashen AF, Dehdashti F, Luo J, Homb A, Siegel BA, Bartlett NL. ^{18}F-FDG PET/CT for early response assessment in diffuse large B-cell lymphoma: poor predictive value of international

harmonization project interpretation. J Nucl Med 2011; 52: 386–392. doi:10.2967/jnumed.110.082586. PMid:21321279.

[6] Chan SC, Wang HM, Yen TC, et al. (18)F-FDG PET/CT and 3.0-T whole-body MRI for the detection of distant metastases and second primary tumours in patients with untreated oropharyngeal/hypopharyngeal carcinoma: a comparative study. Eur J Nucl Med Mol Imaging 2011; 38: 1607–1619. doi:10.1007/s00259-011-1824-y. PMid:21567252.

[7] Di Cesare E, Cerone G, Enrici RM, Tombolini V, Anselmo P, Masciocchi C. MRI characterization of residual mediastinal masses in Hodgkin's disease: long-term follow-up. Magn Reson Imaging 2004; 22: 31–38. doi:10.1016/j.mri.2003.08.002. PMid:14972392.

[8] Rahmouni A, Tempany C, Jones R, Mann R, Yang A, Zerhouni E. Lymphoma: monitoring tumor size and signal intensity with MR imaging. Radiology 1993; 188: 445–451. PMid:8327695.

[9] Koh DM, Collins DJ. Diffusion-weighted MRI in the body: applications and challenges in oncology. AJR Am J Roentgenol 2007; 188: 1622–1635. doi:10.2214/AJR.06.1403. PMid:17515386.

[10] Thoeny HC, Ross BD. Predicting and monitoring cancer treatment response with diffusion-weighted MRI. J Magn Reson Imaging 2010; 32: 2–16. doi:10.1002/jmri.22167. PMid:20575076.

[11] Gu J, Chan T, Zhang J, Leung AY, Kwong YL, Khong PL. Whole-body diffusion-weighted imaging: the added value to whole-body MRI at initial diagnosis of lymphoma. AJR Am J Roentgenol 2011; 197: W384–391. doi:10.2214/AJR.10.5692. PMid:21862763.

[12] Vandecaveye V, De Keyzer F, Nuyts S, et al. Detection of head and neck squamous cell carcinoma with diffusion weighted MRI after (chemo)radiotherapy: correlation between radiologic and histopathologic findings. Int J Radiat Oncol Biol Phys 2007; 67: 960–971. doi:10.1016/j.ijrobp.2006.09.020. PMid:17141979.

[13] Takahara T, Imai Y, Yamashita T, Yasuda S, Nasu S, Van Cauteren M. Diffusion weighted whole body imaging with background body signal suppression (DWIBS): technical improvement using free breathing, STIR and high resolution 3D display. Radiat Med 2004; 22: 275–282. PMid:15468951.

[14] Kwee TC, Takahara T, Ochiai R, et al. Complementary roles of whole-body diffusion-weighted MRI and ^{18}F-FDG PET: the state of the art and potential applications. J Nucl Med 2010; 51: 1549–1558. doi:10.2967/jnumed.109.073908. PMid:20847177.

[15] Mürtz P, Krautmacher C, Träber F, Gieseke J, Schild HH, Willinek WA. Diffusion-weighted whole-body MR imaging with background body signal suppression: a feasibility study at 3.0 Tesla. Eur Radiol 2007; 17: 3031–3037.

[16] Lin C, Itti E, Luciani A, et al. Whole-body diffusion-weighted imaging with apparent diffusion coefficient mapping for treatment response assessment in patients with diffuse large B-cell lymphoma: pilot study. Invest Radiol 2011; 46: 341–349. PMid:21263330.

[17] Wu X, Kellokumpu-Lehtinen PL, Pertovaara H, et al. Diffusion-weighted MRI in early chemotherapy response evaluation of patients with diffuse large B-cell lymphoma - a pilot study: comparison with 2-deoxy-2-fluoro-D-glucose-positron emission tomography/computed tomography. NMR Biomed 2011; 24: 1181–1190. doi:10.1002/nbm.1689. PMid:21387451.

[18] Mürtz P, Kaschner M, Träber F, et al. Evaluation of dual-source parallel RF excitation for diffusion-weighted whole-body MR imaging with background body signal suppression at 3.0T. Eur J Radiol 2011; 81: 3614–3623.

[19] Vandecaveye V, Dirix P, De Keyzer F, et al. Predictive value of diffusion-weighted magnetic resonance imaging during chemoradiotherapy for head and neck squamous cell carcinoma. Eur Radiol 2010; 20: 1703–1714. doi:10.1007/s00330-010-1734-6. PMid:20179939.

[20] Front D, Israel O. The role of Ga-67 scintigraphy in evaluating the results of therapy of lymphoma patients. Semin Nucl Med 1995; 25: 60–71. PMid:7716559.

[21] Vose JM, Bierman PJ, Anderson JR, et al. Single-photon emission computed tomography gallium imaging versus computed tomography: predictive value in patients undergoing high-dose chemotherapy and autologous stem-cell transplantation for non-Hodgkin's lymphoma. J Clin Oncol 1996; 14: 2473–2479. PMid:8823325.

[22] Afaq A, Andreou A, Koh DM. Diffusion-weighted magnetic resonance imaging for tumour response assessment: why, when and how? Cancer Imaging 2010; 10: S179–188. doi:10.1102/1470-7330.2010.9032. PMid:20880779.

[23] Arlinghaus LR, Li X, Levy M, et al. Current and future trends in magnetic resonance imaging assessments of the response of breast tumors to neoadjuvant chemotherapy. J Oncol 2010; 919620; doi:10.1155/2010/919620. PMid:20953332.

[24] Bonekamp S, Jolepalem P, Lazo M, Gulsun MA, Kiraly AP, Kamel IR. Hepatocellular carcinoma: response to TACE assessed with semiautomated volumetric and functional analysis of diffusion-weighted and contrast-enhanced MR imaging data. Radiology 2011; 260: 752–761. doi:10.1148/radiol.11102330. PMid:21771960.

[25] Cui Y, Zhang XP, Sun YS, Tang L, Shen L. Apparent diffusion coefficient: potential imaging biomarker for prediction and early detection of response to chemotherapy in hepatic metastases. Radiology 2008; 248: 894–900. doi:10.1148/radiol.2483071407. PMid:18710982.

[26] Hayashida Y, Yakushiji T, Awai K, et al. Monitoring therapeutic responses of primary bone tumors by diffusion-weighted image: initial results. Eur Radiol 2006; 16: 2637–2643. doi:10.1007/s00330-006-0342-y. PMid:16909220.

[27] Moffat BA, Chenevert TL, Meyer CR, et al. The functional diffusion map: an imaging biomarker for the early prediction of cancer treatment outcome. Neoplasia 2006; 8: 259–267. doi:10.1593/neo.05844. PMid:16756718.

[28] Patterson DM, Padhani AR, Collins DJ. Technology insight: water diffusion MRI–a potential new biomarker of response to cancer therapy. Nat Clin Pract Oncol 2008; 5: 220–233. doi:10.1038/ncponc1073. PMid:18301415.

[29] Huang MQ, Pickup S, Nelson DS, et al. Monitoring response to chemotherapy of non-Hodgkin's lymphoma xenografts by T(2)-weighted and diffusion-weighted MRI. NMR Biomed 2008; 21: 1021–1029. doi:10.1002/nbm.1261. PMid:18988250.

[30] Wu X, Korkola P, Pertovaara H, Eskola H, Järvenpää R, Kellokumpu-Lehtinen PL. No correlation between glucose metabolism and apparent diffusion coefficient in diffuse large B-cell lymphoma: a PET/CT and DW-MRI study. Eur J Radiol 2011; 79: e117–e121. doi:10.1016/j.ejrad.2011.04.062. PMid:21596501.

[31] Reischauer C, Froehlich JM, Koh DM, et al. Bone metastases from prostate cancer: assessing treatment response by using diffusion-weighted imaging and functional diffusion maps–initial observations. Radiology 2010; 257: 523–531. doi:10.1148/radiol.10092469. PMid:20829534.

[32] Horger M, Weisel K, Horger W, Mroue A, Fenchel M, Lichy M. Whole-body diffusion-weighted MRI with apparent diffusion coefficient mapping for early response monitoring in multiple myeloma: preliminary results. AJR Am J Roentgenol 2011; 196: W790–795. doi:10.2214/AJR.10.5979. PMid:21606271.

[33] Takahara T, Kwee T, Kibune S, et al. Whole-body MRI using a sliding table and repositioning surface coil approach. Eur Radiol 2010; 20: 1366–1373. doi:10.1007/s00330-009-1674-1. PMid:19997846.